

Defect mediated optical detection of ammonia using SnO₂ nanoparticle

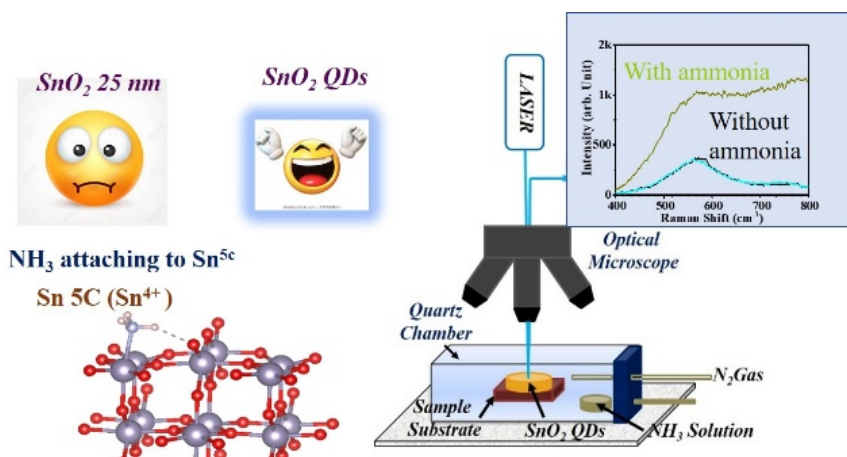
Binaya Kumar Sahu,^{1,3} Gurpreet Kaur,² Arindam Das,^{1*}

¹Surface and Nanoscience Division, Materials Science Group, Indira Gandhi Centre for Atomic Research, Homi Bhabha National Institute, Kalpakkam 603102, India. ²Materials Physics Division, Materials Science Group, Indira Gandhi Centre for Atomic Research, Kalpakkam 603102, India. ³School of Physical Sciences, National Institute of Science Education and Research, Homi Bhabha National Institute, Bhubaneswar, Odisha 752050, India.

Submitted on: 08-Nov-2021 Accepted and Published on: 28-Jan-2022

ABSTRACT

SnO₂, an *n*-type semiconductor used commercially as resistive sensors at high temperature suffers from drifting voltage, contact resistances and poor selectivity. On the other hand, excellent optical property arising from defects in rutile SnO₂ offers opportunities that remain to be explored for optical gas sensor applications. During optical detection, besides the advantage of contact and voltage less measurement, excitation with different light energy can further tune the sensing ability. Thus, it has enormous scopes to provide an improved sensor response and selectivity. In this direction, we report the synthesis and characterization of SnO₂ nanostructures with an emphasis on their Raman and photoluminescence properties. The crucial role of defects for the improved optical responses and selectivity for ammonia is highlighted along with a plausible mechanism.



Keywords: Optical detection, Ammonia, Quantum Dots, Raman, Photoluminescence

INTRODUCTION

In recent times, tremendous efforts have been given for designing and developing efficient gas sensors to be used for monitoring health, environmental and industrial safety.^{1,2} In fact, conventional thin-film resistive sensors have attained commercial success with low detection limit and high selectivity. Mostly, these resistive sensors operate at an elevated temperature of 300 °C or higher to supply the required activation energy for the chemisorption reactions taking place at surfaces with oxygen

moieties.^{3,4} The high-temperature operation not only affects the sensor integrations, it also becomes high energy demanding and costly system. So, the demand for alternative sensing strategies at or near room temperature attracts considerable research attention. One of the options is the optical probe which provides a reasonably measurable change in the response signal in the presence of analytes.^{5,6} Apart from the possible low-temperature operation, it offers other benefits such as enhanced selectivity, portability and contactless sensing. In that direction, metal oxide nanostructures (NSs) are found to be a crucial component considering the availability of huge surface areas as well as outstanding optical properties from the varied defects states.

As a wide bandgap semiconductor, SnO₂ nanostructure has attracted immense interest because of its potential uses in optical devices and electrical appliances.⁷⁻¹¹ The properties of SnO₂ depend on nanostructure morphologies and electronics structures which are modified by the intrinsic oxygen vacancies (OV). Earlier, we have demonstrated also the evolution of varied optical properties in

*Corresponding Author: Dr. Arindam Das, Surface and Nanoscience Division, Materials Science Group, Indira Gandhi Centre for Atomic Research, Homi Bhabha National Institute, Kalpakkam 603102, India
Email: dasa@igcar.gov.in



different nanostructures such as nanowires, tetragonal microcubes, nanoribbon and nanocrystals (NCs) and their potent applications like gas sensing, waveguide, supercapacitor and catalysis.^{12,13} Moreover, recently optical sensing of ammonia using SnO₂ NPs was depicted where photo-induced luminescence (PL) technique was used as a probe.¹⁴ In this study, the blue region of PL spectra was found to be elevated in the presence of ammonia vapor. The role of various OV and the Lewis acid-base interaction was forwarded as a mechanism for selective PL-based ammonia sensing using QDs.¹⁴ The results aspire further to investigate the sensing study by combining both the Raman and PL measurements. It is important to mention that during the PL measurement, the Raman signal may appear due to overlap of the energy scale. Importantly, the Raman spectra provide important information on the presence of various OV in SnO₂ NPs. So, the effective change of PL and Raman spectra in a single frame during an interaction with ammonia will unfold better insights and the detailed mechanism. In addition, excitations of sensing material with various lasers would unfurl detailed optical properties. For instance, the excitation of SnO₂ with the UV and the visible sources will explore different optical regimes.¹⁵ In addition to OV, the presence of hydroxyl group (-OH) was illustrated as a crucial defect on the surfaces of NPs to influence the sensing performances.¹⁵ Notably, the presence of these -OH groups is probed easily by both infrared and Raman spectroscopy. Hence it opens up the possibility of observation of the specific role of -OH groups during ammonia sensing.

The report carries an elucidation of the interaction mechanism of ammonia at various active sites in SnO₂ nanoparticles and it includes spectroscopic evidence and theoretical supports. Firstly, analysis of different defects in SnO₂ using Raman spectroscopy with 325 and 532 nm laser excitations is highlighted. Systematic emission property is also carried out for understanding the defect-related optical properties. The presence of the -OH group, along with its possible interaction with ammonia, is corroborated using both FTIR and Raman measurements. Then, the scope of optical-based ammonia sensing at room temperature is demonstrated. Furthermore, the selectivity of ammonia among other volatile gases and the typical role of certain defects and their distributions in SnO₂ NPs are presented. In addition, the proposed mechanism for ammonia sensing is augmented with the density functional theory (DFT).

EXPERIMENTAL

SnO₂ nanoparticles (NPs) were prepared through a chemical method by using SnCl₄ and NH₄OH as precursors. The details of the synthesis of NPs were depicted in our previous report.¹⁴ The as-prepared NP was annealed to obtain improved crystalline particles of size ~ 25 nm. X-ray diffraction (XRD) measurement using Cu-K α radiations ($\lambda=0.15406$ nm) and transmission electron microscopy (TEM, Libra 200 Zeiss) were employed for the structural characterization of the as-prepared and annealed samples. Raman spectra were recorded using the Renishaw In-Via spectroscopy in backscattering geometry. Both Ar ion-based 514.5 nm and a He-Cd-based 325 nm laser excitations were employed for Raman measurements to acquire insights about the presence and distribution of defects in SnO₂ NPs. Optical emission was obtained

using a 300 nm excitation source for both particles. Fourier transform infrared spectroscopy (FTIR, Bruker IFS66.) was used for SnO₂ NPs.

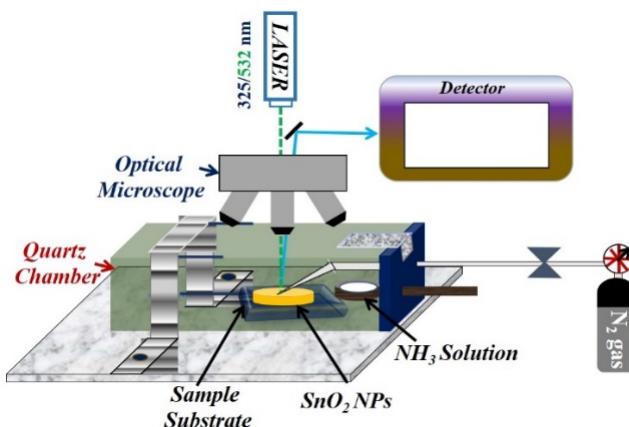


Figure 1. Schematic diagram of the quartz chamber used for the collection of PL signals with an optical microscope and CCD detector

In order to perform PL monitored sensing measurement, a compatible quartz-based chamber was utilized. It is schematically shown in figure 1. Ammonia solution (~50 μ L) of different concentrations (3.125, 1.55, 0.781, 0.39, and 0%) was kept inside the quartz cuvette as a source of ammonia gas. The corresponding amount is then converted and found to be 256, 128, 64, 32 and 0 ppm of ammonia. Details are described in our earlier report.¹⁴ In the presence and absence of NH₃ solution, two different laser excitations of 325 and 514.5 nm were used for collecting data.

For gaining an insight into the selective interaction of NH₃ with the prevailing defects in SnO₂ NSs, first-principles-based density functional theory (DFT) calculations are employed using VASP[r1] (Vienna ab-initio simulation package) with a plane-wave basis set. The interaction between the electrons and nucleus is described using the projector augmented wave method (PAW). For exchange-correlation, a functional rev-PBE version of generalized gradient approximation (GGA) was used. An energy cutoff of 500 eV is found to give total energy convergence of better than 1 meV/atom. Brillouin zone is sampled using 5X5X1 k-point mesh with a total energy tolerance of 10⁻⁸ eV used for reaching SCF. All structures are relaxed until the force on each atom is less than 0.005eV/atom. A slab of SnO₂ oriented in [110] direction having four layers and 48 atoms are created and fully relaxed. To study the interaction with NH₃, two probable sites (Sn⁴⁺ and Sn²⁺) are chosen on the [110] surface of the SnO₂ slab. Change density difference is plotted for both cases.

RESULT AND DISCUSSION

X-ray diffraction patterns were recorded for the range of $2\theta=20$ to 80° for NPs. Results are depicted in figure 2 (a). The patterns are found to match with the standard power diffraction card as given in ICDD 00-041-1445. All the observed diffractions confirmed the rutile tetragonal phase of SnO₂ with no noticeable impurity peaks.⁹ The highly broadened diffractions for the as-prepared compared to sharp features from the annealed sample indicate the presence of two different crystallite sizes. The Scherrer formula provided the

average crystallite sizes of the as-prepared and annealed samples as ~2.4 and 25 nm, respectively.¹³

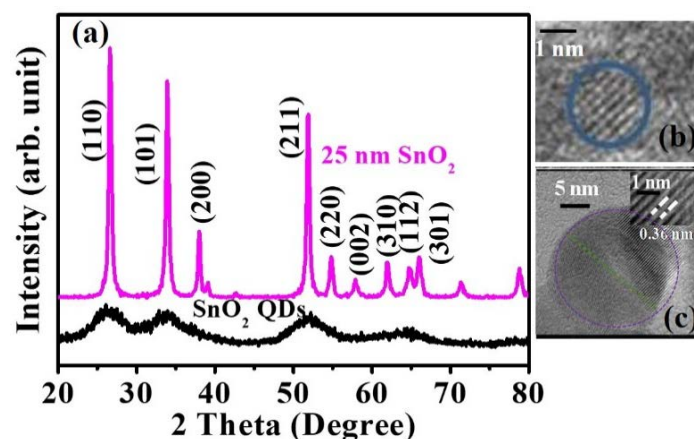


Figure 2. (a) XRD of both SnO₂ NPs, TEM image of (b) QDs and (c) annealed SnO₂

The crystallite sizes are also well supported by the high-resolution TEM images, as shown in Figures 2 (b) and (c). The details of HRTEM were discussed in our earlier report.¹⁶ The smaller size of the as-prepared sample than the reported Bohr exciton of 2.7 nm indicates the formation of quantum dots (QDs) SnO₂, which has shown also a blue-shifted optical band gap value as high as 4.1 eV from the bulk value of 3.6 eV.¹³

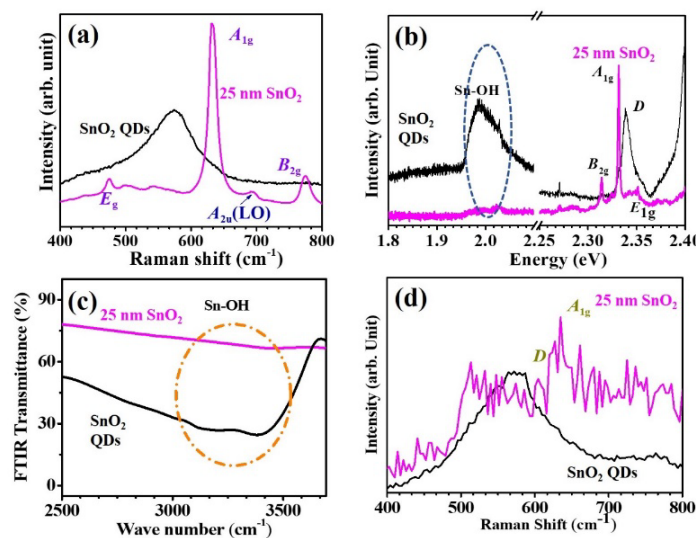


Figure 3. (a) Raman and (b) PL spectra collected 514.5 nm (c) FTIR spectra indicating presence of Sn-OH vibration and (d) Raman spectra collected using 325 nm laser from for SnO₂ NPs

Raman spectroscopy congregates information about the local structure and crystal surface areas. It is used to investigate the structural properties along with defect distributions in SnO₂ NPs by different laser excitations. The results are depicted in figure 3. The SnO₂ tetragonal rutile phase belongs to the D_{4h}^{14} space group and three Raman active modes, E_g , A_{1g} , and B_{2g} are mostly found for the

well-crystallized NPs. Figure 3 (a) depicts Raman spectra collected from QDs and 25 nm using 514.5 nm laser excitation.^{17,18} A sharp peak at 633 cm⁻¹ and a relatively weak peak at 774 cm⁻¹ are seen for 25 nm SnO₂ NPs. These Raman modes indicate the presence of a rutile crystalline phase. In comparison, no such Raman mode is seen for the as-prepared QDs which have a broad peak at 573 cm⁻¹ (D). The D peak arises from surface defects of SnO₂ QDs^{17,19} and such surface defects are very high in QDs compared to the annealed NPs. This distribution of defects is attributed to a higher surface-to-volume ratio for the as-prepared sample. The PL from both the particles using 532 nm excitation is shown in figure 3(b). The Raman allowed mode from -OH moiety is observed strongly for QDs and absent for 25 nm particles.¹⁵ Thus, high-temperature growth affects the -OH modes and does not allow its formation appreciably on its surfaces. This observation is further supported by the FTIR investigation, as shown in Figure 3(c). Raman spectra collected from NPs using 325 nm excitations are shown in Fig. 3(d). For the bigger particle, the Raman allowed A_{1g} peak is observed, whereas, the D peak only appears for the QDs

Figure 4 shows the emission spectra of NPs for 300 nm excitation. The emission property in figure 4 is found to be completely different for QDs and 25 nm SnO₂. Both NPs demonstrate a broad PL peak at ~600 nm, which corresponds to the excitation of the bulk oxygen vacancy-related energy states.²⁰ However, two extra peaks can also be seen at 416 and 435 nm for QDs only. These emission peaks at the higher energy side called the blue region to corroborate the presence of the under coordinated Sn atom [Sn^{4c}] at the surfaces due to loss of oxygen.²¹ In our previous report, a detailed interpretation is given for the origin of the blue peak using a synchrotron-based X-ray absorption spectroscopy (XAS).^{14,22} In that report, the pre-edge spectra exclusively from QDs are correlated with blue luminescence.

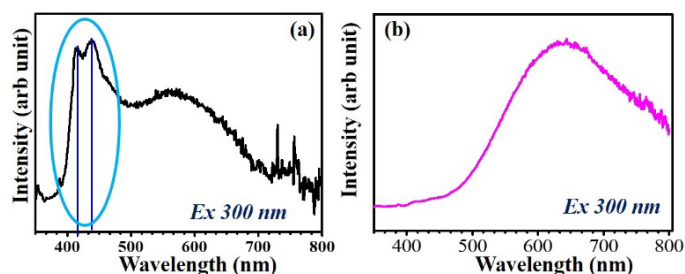


Figure 4. Emission scan collected from SnO₂ (a) QDs and (b) 25 nm with 300 nm excitation

In summary, SnO₂ NPs with two different dimensions and defect distribution is synthesized. It is obvious that due to smaller volume, QDs possess a very high surface area compared to 25 nm particles. The detailed optical characterization revealed that the QD possesses a high volume of surface defects. It is worth mentioning that in SnO₂, Sn with octahedral geometry is surrounded by six oxygen atoms and hence six coordinated (Sn_{6c}). Interestingly, the formation of bulk oxygen vacancy creates an energy state close to the conduction band and contributes n -type conductivity to the system. However, at the surfaces, defects create undercoordinated geometry with Sn⁴⁺ (5c) or Sn²⁺ (4c).^{14,21} Importantly, these surface defects create an energy state close to the valence band and are

generally optically active. However, it hardly contributes to the system's conductivity. With a very high surface area, the contributions from Sn^{4+} and Sn^{2+} defects states are higher for QDs. Observation of the blue luminescence in the emission spectrum of QDs supports the proposition. The next section discusses the interaction of ammonia with these defect sites and their successive impact on the optical property.

To enumerate the interaction of NH_3 with SnO_2 NPs, Raman spectra were collected using 325 nm laser excitation from SnO_2 QDs in the presence and the absence of NH_3 and results are shown in Figure 5. It is observed that there is a strong change in the Raman signal, more prominently beyond the 500 cm^{-1} in the presence of ammonia. Noticeably, such change in intensity is limited only for QDs compared to 25 nm SnO_2 (Figure 5b). For understanding any role of excitation energy for the observed change in the Raman spectra in presence of ammonia, the same experiment was carried out with 514.5 nm laser excitation. The results are presented in Figure 5(c) and (d) for QDs and 25 nm particles, respectively. Here Raman spectra collected from both QDs and 25 nm particles did not undergo noticeable alteration in the presence of ammonia. Thus, the change in the Raman signal in Figure 5a is not only from the true Raman scatterings. So, a possible PL background can cause the appearance of the QDs in the presence of ammonia. For the concrete evidence for the observation of a Raman signal during the 325 nm, Laser excitation for PL measurement is depicted and discussed in the supplementary information Figure SI 1(a). It is worth noticing that the Raman signal depicted by the dotted line in Figure 5(a) indicates the recovery to its original state by removing the ammonia exposure with N_2 purge. Thus, the influence of NH_3 has been ascertained as well as the recovery of active sensor material after withdrawing analyte is also established. For conclusive observation, the PL from QDs in the presence and absence of ammonia under 325 nm excitation is presented in Figure 6a.

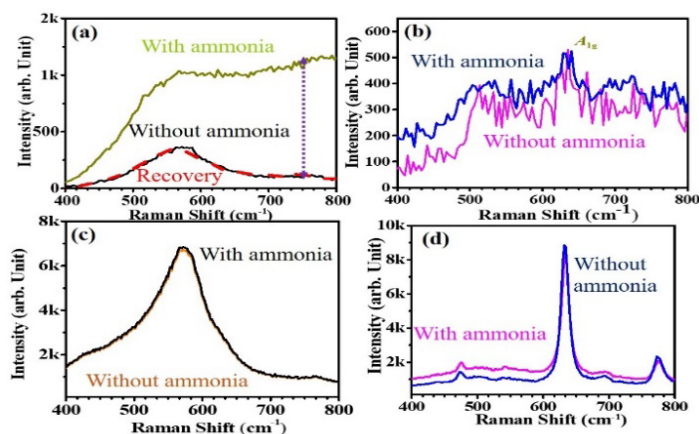


Figure 5. Raman spectra in absence and presence of ammonia collected from (a) QDs, (b) 25 nm with 325 nm laser excitation and (c) QDs, (d) 25 nm SnO_2 with 514.5 nm laser excitation

SnO_2 surfaces contain both Sn^{4+} and Sn^{2+} charges on the surface and act as interacting sites for ammonia. These sites, known as Lewis acid, interact with Lewis base ammonia, via the Lewis-acid base interaction mechanism.^{23–25} Additionally, the critical role of

other moieties such $-\text{OH}$, which is found to be present (Figure 3(b)) on SnO_2 QDs is also probable for interaction with ammonia. To explore it, the Raman measurement like in Figure 3(b) is further scrutinized with ammonia exposures. The result is shown in Figure 6. Along with the D peak from the SnO_2 QDs, the signature of $-\text{OH}$ is also clearly seen in Figure 6(b) when the material is excited with a laser exciton of 514.5 nm. On the exposure to ammonia, the $-\text{OH}$ signature is retained with no significant alteration (Figure 6b). So, no pertinent change indicates that the hydroxyl group has a limited role in displaying the PL signature as seen in Figure 6a with ammonia.

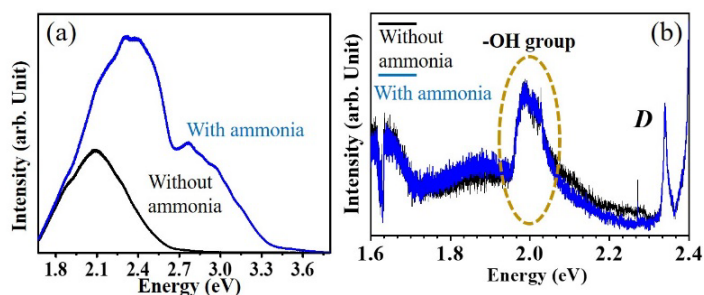


Figure 6. (a) PL from SnO_2 QDs in absence and presence of ammonia (b) Depicting unaltered $-\text{OH}$ group of SnO_2 QDs in the presence of ammonia with 514.5 laser excitation for PL measurement.

However, a dedicated study earlier by our group has demonstrated the detachment of the $-\text{OH}$ group by temperature treatment.¹³ Presently, equivalent treatment by the UV Laser treatment can cause similar detachment. Hence during the Raman measurement, it is most likely that the $-\text{OH}$ group will be detached from SnO_2 NPs and both Sn^{2+} and Sn^{4+} are then exposed to ammonia for interaction. This is shown in the schematic plot in Figure 7 (a).

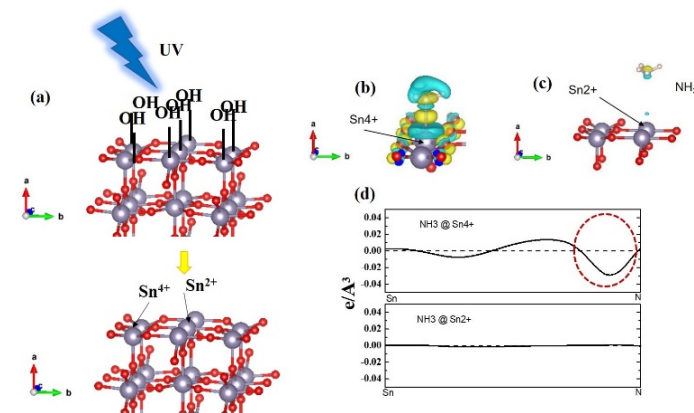


Figure 7. (a) Showing schematic of removal of $-\text{OH}$ group due to UV exposure. Charge density iso-surface plot from DFT studies for the interaction of NH_3 with (b) Sn^{4+} (c) Sn^{2+} and (d) line charge profile in between SnO_2 and NH_3 .

Successive removal of the $-\text{OH}$ group creates two competitive sites Sn^{2+} and Sn^{4+} to attract ammonia. In that direction, our DFT study pointed to further insights regarding the surface chemistry, including charge distribution of adsorption configurations as

depicted in Figure 7 (b), (c) and (d). The isosurface plots for the reduced SnO₂ surface show bonding of NH₃ to Sn⁴⁺ and no bonding in the case of Sn²⁺ [Figure 7(b) and (c)]. Further Figure 7(d) shows the line charge profile between Sn from SnO₂ surface and N of NH₃. There is a clear indication of the concentration of charge in the centre of N and Sn⁴⁺ showing the interaction of NH₃ and Sn⁴⁺ whereas for the case of Sn²⁺, there is an almost negligible variation of charge in between Sn²⁺ and NH₃, and there is no interaction.

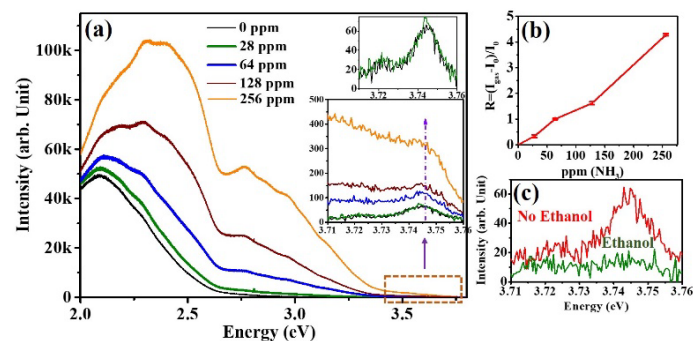


Figure 8. (a) PL of QDs in different concentration ammonia (bottom inset) corresponding change in Raman intensity (top inset) for 0 and 28 ppm (b) Sensor response (c) Raman intensity in the presence of ethanol.

Further, for testing sensitivity with QDs, different concentrations of ammonia are allowed to interact. The results are described in Fig. 8(a). The PL signature changes with the increase of ammonia concentration. Interestingly, the Raman region from PL spectra as shown in Fig 8(a) (bottom inset) shows a systemic variation with ammonia concentration. A minute change in intensity at 28 ppm is also depicted in Figure 8(a) (top inset). The response is defined by the formula $R = (I_{gas} - I_0) / I_0$. Where I_{gas} and I_0 are the intensities of Raman peak as shown in Figure 8(a) (bottom inset). The response curve is shown in Figure 8(b) and almost a linear response is recorded. For selectivity, a similar measurement is carried out in the presence of ethanol and depicted in Figure 8(c). Here a reduction in the Raman intensity is noticed in the presence of ethanol, which is markedly different from the response in presence of ammonia which shows an increased Raman intensity. Thus, a selective interaction is established among volatile analytes such as alcohols.

A clear alteration in the Raman spectra due to enhancement in the PL background from SnO₂ QDs is observed in the presence of ammonia. Such change can be taken as a sensor output. In addition, such a change in optical signal is well supported by the DFT study.

CONCLUSION

An alternative mode of sensing, photoluminescence (PL) sensor performance, is demonstrated by using SnO₂ quantum dots (QDs) and compared with relatively bigger particles. Optically active defects are exploited in a single frame using both Raman and PL spectroscopy in a single frame. For the prevailing mechanism, defects induced PL in the SnO₂ nanoparticles (NPs) is discussed with crucial inferences with emphasis on truncated Sn atoms and hydroxyl group present on the surface over the typical oxygen vacancies. Further correlating uncoordinated multivalent Sn as Lewis acid interaction sites for basic NH₃ and subsequent increase

in luminescence background in Raman spectra is unfolded and explored experimentally with theoretical inputs using iso charge surface and line distribution charge by the density functional theory (DFT) calculations. Thus, beyond the superlative performance of the PL sensor using optical defects in the SnO₂ QDs, the explored mechanism is of high significance, which sets up a novel platform for the defects engineering-based optoelectronic applications.

ACKNOWLEDGMENTS

We thank S. Amirthapandian and P. Magudapathy (MSG/IGCAR) for TEM and XRD studies, respectively. The authors are grateful to Sandip Dhara (MSG/IGCAR) for useful discussions.

CONFLICT OF INTEREST

Authors declared no conflict of interest exist.

REFERENCES AND NOTES

- P. Sun, Y. Cai, S. Du, et al. Hierarchical α -Fe₂O₃/SnO₂ semiconductor composites: Hydrothermal synthesis and gas sensing properties. *Sensors Actuators, B Chem.* **2013**, 182, 336–343.
- A. Maiti, J.A. Rodriguez, M. Law, et al. SnO₂ nanoribbons as NO₂ sensors: Insights from first principles calculations. *Nano Lett.* **2003**, 3 (8), 1025–1028.
- S.S. Kim, H.G. Na, H.W. Kim, V. Kulish, P. Wu. Promotion of acceptor formation in SnO₂ nanowires by e-beam bombardment and impacts to sensor application. *Sci. Rep.* **2015**, 5.
- H.C. Su, M. Zhang, W. Bosze, N. V. Myung. Tin Dioxide Functionalized Single-Walled Carbon Nanotube (SnO₂/SWCNT)-Based Ammonia Gas Sensors and Their Sensing Mechanism. *J. Electrochem. Soc.* **2014**, 161 (14), B283–B290.
- E.S.M. Duraia, S. Das, G.W. Beall. Humic acid nanosheets decorated by tin oxide nanoparticles and their humidity sensing behavior. *Sensors Actuators, B Chem.* **2019**, 280, 210–218.
- D. Valerini, A. Cretì, A.P. Caricato, et al. Optical gas sensing through nanostructured ZnO films with different morphologies. *Sensors Actuators, B Chem.* **2010**, 145 (1), 167–173.
- T. Kim, V.G. Parale, H.N.R. Jung, et al. Facile synthesis of SnO₂ aerogel/reduced graphene oxide nanocomposites via in situ annealing for the photocatalytic degradation of methyl orange. *Nanomaterials* **2019**, 9 (3).
- V. Bonu, B.K. Sahu, A. Das, et al. Sub-wavelength waveguide properties of 1D and surfacefunctionalized SnO₂ nanostructures of various morphologies. *Beilstein J. Nanotechnol.* **2019**, 9 (1), 379–388.
- B.K. Sahu, A. Das. Significance of in-plane oxygen vacancy rich non-stoichiometric layer towards unusual high dielectric constant in nanostructured SnO₂. *Phys. E Low-Dimensional Syst. Nanostructures* **2018**, 103, 60–65.
- S.B. Kondawar, A.M. More, H.J. Sharma, S.P. Dongre. Ag-SnO₂/Polyaniline composite nanofibers for low operating temperature hydrogen gas sensor. *J. Mater. Nanosci.* **2017**, 4 (1), 13–18.
- M. Jouyandeh, S.S. Mousavi Khadem, S. Habibzadeh, et al. Quantum dots for photocatalysis: synthesis and environmental applications. *Green Chem.* **2021**, 23 (14), 4931–4954.
- B.K. Sahu, A. Das. Graphene oxide surface chemistry regulated growth of SnO₂ nanoparticles for electrochemical application. *J. Alloys Compd.* **2020**, 834.
- B.K. Sahu, A. Das. Significance of oxygen defects in SnO₂ quantum dots as hybrid electrochemical capacitors. *J. Phys. Chem. Solids* **2019**, 129, 293–297.
- B.K. Sahu, A. Das, G. Kaur. Revealing interplay of defects in SnO₂ quantum dots for blue luminescence and selective trace ammonia detection at room temperature. *ACS Appl. Mater. Interfaces* **2020**, 12 (43), 49227–49236.
- V. Bonu, A. Das, S. Amirthapandian, S. Dhara, A.K. Tyagi. Photoluminescence of oxygen vacancies and hydroxyl group surface

- functionalized SnO₂ nanoparticles. *Phys. Chem. Chem. Phys.* **2015**, 17 (15), 9794–9801.
16. K.K. Mishra, B.K. Sahu, V. Bonu, et al. Raman Fingerprint of Pressure-Induced Phase Transition in SnO₂ Nanoparticles: Grüneisen Parameter and Thermal Expansion. *J. Phys. Chem. C* **2021**, 125 (42), 23287–23298.
 17. A. Diéguez, A. Romano-Rodríguez, A. Vilà, J.R. Morante. The complete Raman spectrum of nanometric SnO₂ particles. *J. Appl. Phys.* **2001**, 90 (3), 1550–1557.
 18. L.P. Ravaro, L.V.A. Scalvi, A.S. Tabata, F.M.L. Pontes, J.B.B. Oliveira. Nanoparticle characterization of Er-doped SnO₂ pellets obtained with different pH of colloidal suspension. *J. Appl. Phys.* **2013**, 114 (8).
 19. L.Z. Liu, J.Q. Xu, X.L. Wu, et al. Optical identification of oxygen vacancy types in SnO₂ nanocrystals. *Appl. Phys. Lett.* **2013**, 102 (3).
 20. V. Bonu, A. Das, A.K. Prasad, et al. Influence of in-plane and bridging oxygen vacancies of SnO₂ nanostructures on CH₄ sensing at low operating temperatures. *Appl. Phys. Lett.* **2014**, 105 (24).
 21. S. Ghosh, K. Das, K. Chakrabarti, S.K. De. Effect of oleic acid ligand on photophysical, photoconductive and magnetic properties of monodisperse SnO₂ quantum dots. *J. Chem. Soc. Dalton Trans.* **2013**, 42 (2), 3434–3446.
 22. Q. Zhu, Q. Ma, D.B. Buchholz, et al. Structural anisotropy in amorphous SnO₂ film probed by X-ray absorption spectroscopy. *Appl. Phys. Lett.* **2013**, 103 (3).
 23. A. V. Marikutsa, M.N. Romyantseva, A.M. Gaskov, A.M. Samoylov. Nanocrystalline tin dioxide: Basics in relation with gas sensing phenomena part II. Active centers and sensor behavior. *Inorg. Mater.* **2016**, 52 (13), 1311–1338.
 24. A. V. Marikutsa, M.N. Romyantseva, E.A. Konstantinova, T.B. Shatalova, A.M. Gaskov. Active sites on nanocrystalline tin dioxide surface: Effect of palladium and ruthenium oxides clusters. *J. Phys. Chem. C* **2014**, 118 (37), 21541–21549.
 25. M.N. Alaya, M.A. Rabah. Surface acidity and catalytic activity of aged SO₂/SnO₂ catalyst supported with WO₃. *J. Alloys Compd.* **2013**, 575, 285–291.